Conclusion. Distal steric effects in anthracene heme cyclophanes and other cyclophanes can be large. They reside almost exclusively in the ligand association rates, suggesting a control by a conformational preequilibrium. Distal steric effects differentiate ligands by gross size and shape but do not significantly differentiate linear from bent binding diatomic molecules. Variations in K^{CO}/K^{O_2} are found to be the result of changes in polar rather than steric effects.

Acknowledgment. We are grateful to the National Institutes of Health for support of this work (Grant HL 13581) and for support of the computer applications (Grant RR 00757) and to Prof. C. K. Chang for helpful discussions.

Registry No. **1**, 93985-01-4; **1**-(MeIm), 93985-21-8; **1**-$(MeIm)_2$, 93985-23-0; **1**-(MeIm)(*n*-BuNC), 93985-05-8; **1**-(MeIm)(*t*-BuNC), 93985-06-9; **1**-(MeIm)(TMIC), 93985-07-0; **1**-(MeIm)($C_6H_{11}NC$), 93985-08-1; **1**-(*n*-BuNC), 93985-36-5; **1**-(*t*-BuNC), 93985-24-1; **1**-(TMIC), 93985-25-2; **1**-($C_6H_{11}NC$), 93985-26-3; **1**-$(n\text{-BuNC})_2$, 93985-30-9; **1**-$(t\text{-BuNC})_2$, 94089-29-9; **1**-$(TMIC)_2$, 93985-31-0; **1**-$(C_6H_{11}NC)_2$, 93985-32-1; **1**-(DCIM)(CO), 93985-04-7; **1**-(MeIm)(CO), 93985-18-3; **1**-(1,2-Me_2Im)(CO), 93985-16-1; **1**-(DCIM)(O_2), 94024-66-5; **2**, 93985-02-5; **2**-(DCIM), 93985-22-9; **2**-$(MeIm)_2$, 93985-20-7; **2**-(DCIM)(MeIm), 93985-19-4; **2**-(DCIM)(*n*-BuNC), 93985-09-2; **2**-(DCIM)(*t*-BuNC), 93985-10-5; **2**-(DCIM)(TMIC), 93985-11-6; **2**-(*n*-BuNC), 93985-27-4; **2**-(*t*-BuNC), 93985-28-5; **2**-(TMIC), 93985-29-6; **2**-$(n\text{-BuNC})_2$, 93985-33-2; **2**-$(t\text{-BuNC})_2$, 93985-34-3; **2**-$(TMIC)_2$, 93985-35-4; **2**-(DCIM)(CO), 93985-03-6; **2**-(MeIm)(CO), 93985-17-2; **2**-(1,2-Me_2Im)(CO), 93985-15-0; **2**-(DCIM)(O_2), 94024-65-4; TMIC, 36635-61-7; MeIm, 616-47-7; 1,2-Me_2Im, 1739-84-0; DCIm, 80964-44-9; CO, 630-08-0; O_2, 7782-44-7; *n*-BuNC, 2769-64-4; *t*-BuNC, 7188-38-7; $C_6H_{11}NC$, 931-53-3; $C_6H_{11}NH_2$, 108-91-8; $C_6H_{11}CHO$, 2043-61-0; chelated protoheme, 76747-88-1; chelated protoheme-(*n*-BuNC), 93985-12-7; chelated protoheme-(*t*-BuNC), 93985-13-8; chelated protoheme-(TMIC), 93985-14-9.

Model Studies of Iron-Tyrosinate Proteins

Joseph W. Pyrz, A. Lawrence Roe, Lawrence J. Stern, and Lawrence Que, Jr.*†

Contribution from the Departments of Chemistry, Cornell University, Ithaca, New York 14853, and University of Minnesota, Minneapolis, Minnesota 55455. *Received April 30, 1984*

Abstract: The phenolate-to-iron(III) charge-transfer transition in a series of iron(III) phenolate complexes has been investigated. NMR contact shifts for the phenolate protons are well correlated with the visible absorption maxima of the complexes and the Fe^{III}/Fe^{II} redox potentials. The results indicate that the energy of the phenolate-to-iron(III) charge-transfer band is sensitive to the crystal field strength of the other ligands coordinated to the ferric center. The stronger the other ligands are, the higher the energy of the phenolate charge-transfer band. The blue shift of the charge-transfer band is also reflected in smaller contact shifts for the phenolate protons and a more negative Fe^{III}/Fe^{II} redox potential. On the basis of these studies, the probable identities of ligating species in transient dioxygenase intermediates are deduced. These studies also demonstrate that a square-pyramidal complex with an apical and a basal phenolate can give rise to phenolate charge-transfer bands of quite different energies. A dioxygenase active site approaching such a structure is proposed. Lastly, the axial ligand in Fe(salen)OC_6H_4-4-CH_3 is shown to be an excellent model for tyrosine in resonance Raman studies of iron-tyrosinate proteins. Isotopic substitution studies on the model complex show that the ca. 570-cm^{-1} feature found in these proteins cannot be assigned solely to an Fe-O stretching vibration.

The coordination of tyrosine to metal centers in proteins is a structural feature recently found for a number of metalloproteins.[1] Resonance Raman spectroscopy has played a crucial role in elucidating this coordination feature in the transferrins,[2-5] the catechol dioxygenases,[6-10] and the purple acid phosphatases.[11-13] These comprise the new subclass of iron-tyrosinate proteins.[7] Resonance-enhanced phenolate vibrations observed at ca. 1170, 1270, 1500, and 1600 cm^{-1} result from excitation into the tyrosinate-to-iron(III) charge-transfer bands and are the characteristic Raman spectral signature for these proteins. In several cases, a prominent low-frequency feature near 570 cm^{-1} is also observed[10,12,14] and is proposed to arise from Fe-O modes. To assign this vibration, we have studied the Raman spectrum of a ferric *p*-cresolate complex employing ^{54}Fe, ^{18}O, and ^{2}H isotopic substitutions.

The factors affecting the energy of the phenolate-to-iron(III) charge transfer transition have also been investigated. The tyrosinate-to-iron(III) charge-transfer bands in the proteins are clearly sensitive to the ligand environment, as evidenced by the broad range of colors exhibited by iron-tyrosinate proteins. The charge-transfer transition in Fe(III) transferrins can be shifted simply by changing the Lewis base function on the synergistic anion,[15] while the binding of a variety of substrates and inhibitors to the catechol dioxygenases gives rise to complexes with absorption maxima spanning the 400-600-nm region.[16-20]

Although previous studies have investigated spectral shifts in iron phenolate complexes,[21,22] recent observations on the catechol

† University of Minnesota.

(1) Que, L., Jr. *Coord. Chem. Rev.* **1983**, *50*, 73-108.
(2) Carey, P. R.; Young, N. M. *Can. J. Biochem.* **1974**, *52*, 273-280.
(3) Gaber, B. P.; Miskowski, V.; Spiro, T. G. *J. Am. Chem. Soc.* **1974**, *96*, 6868-6873.
(4) Tomimatsu, Y.; Kint, S.; Scherer, J. R. *Biochemistry* **1976**, *15*, 4918-4924.
(5) Ainscough, E. W.; Brodie, A. M.; Plowman, J. E.; Bloor, S. J.; Loehr, J. S.; Loehr, T. M. *Biochemistry* **1980**, *19*, 4072-4079.
(6) Tatsuno, Y.; Saeki, Y.; Iwaki, M.; Yagi, T.; Nozaki, M.; Kitagawa, T.; Otsuka, S. *J. Am. Chem. Soc.* **1978**, *100*, 4614-4615.
(7) Keyes, W. E.; Loehr, T. M.; Taylor, M. L. *Biochem. Biophys. Res. Commun.* **1978**, *83*, 941-945.
(8) Felton, R. H.; Cheung, L. D.; Phillips, R. S.; May, S. W. *Biochem. Biophys. Res. Commun.* **1978**, *85*, 844-850.
(9) Que, L., Jr.; Heistand, R. H., II *J. Am. Chem. Soc.* **1979**, *101*, 2219-2221.
(10) Bull, C.; Ballou, D. P.; Salmeen, I. *Biochem. Biophys. Res. Commun.* **1979**, *87*, 836-841.
(11) Gaber, B. P.; Sheridan, J. P.; Bazer, F. W.; Roberts, R. M. *J. Biol. Chem.* **1979**, *254*, 8340-8342.
(12) Antanaitis, B. C.; Strekas, T.; Aisen, P. *J. Biol. Chem.* **1982**, *257*, 3766-3770.
(13) Davis, J. C.; Averill, B. A. *Proc. Natl. Acad. Sci. U.S.A.* **1982**, *79*, 4623-4627.
(14) Nagai, K.; Kagimoto, T.; Hayashi, A.; Taketa, F.; Kitagawa, T. *Biochemistry* **1983**, *22*, 1305-1311.
(15) Schlabach, M. R.; Bates, G. W. *J. Biol. Chem.* **1975**, *250*, 2182-2188.
(16) Fujisawa, H.; Uyeda, M.; Kojima, Y.; Nozaki, M.; Hayaishi, O. *J. Biol. Chem.* **1972**, *247*, 4414-4421.

0002-7863/85/1507-0614$01.50/0

Table I. Spectral and Electrochemical Data for Iron–Phenolate Complexes

compd	ν_{max},[a] $\times 10^3$ cm^{-1}	δ[b] 4-H	δ[b] 5-H	δ[b] 6-H	$E°'$, [ΔE_p, mV][c]	ref
Fe(salen)I	19.6	83.1	−74.2	56.1	−0.328 [113]	26
Fe(salen)Br	20.2	81.4	−71.3	52.8	−0.468 [103]	27
Fe(salen)Cl	21.6	79.1	−67.9	49.7	−0.610 [88]	28
Fe(salen)OAc	20.8	77.3	−67.4	48.3	−0.811 [82]	29
Fe(salen)SPh	22.7	76.0	−69.0	50.0	−0.777 [69]	29
Fe(salen)OC_6Cl_5	23.0	75.8	−62.6	47.1		29
Fe(salen)OC_6H_2-2,4,6-Cl_3	23.2	74.5	−60.1	46.1	−0.732 [109]	29
Fe(salen)OC_6H_4-X						
X = 4-NO_2		73.0	−57.6	44.3		29
X = 4-CN	23.6	72.5	−56.4	43.9		29
X = 4-CF_3	24.3	72.0	−55.2	43.5		29
X = 4-$COCH_3$	24.4	72.1	−55.3	43.7		29
X = 4-F	24.8	70.5	−52.5	42.4		29
X = 4-Cl	24.4	71.0	−53.5	42.8		29
X = 2-Cl	24.0	71.6	−54.7	43.2	−0.859 [101]	29
X = 2-Br	24.3	71.2	−54.5	43.0	−0.848 [105]	29
X = H	24.4	70.2	−51.7	42.1	−0.924 [90]	29
X = 4-CH_3	24.4	69.5	−51.0	41.8		29
X = 4-OCH_3	24.9	69.5	−50.6	41.7		29
Fe(salen)DBcatH	23.9	71.4	−54.3	43.6		29
Fe(salen)PD^-	27.5/32.1	56.8	−32.4	25.0	−1.711 [104]	30
Fe(salen)$DBcat^-$	26.2/29.5	54.4	−32.0	25.0	−1.841 [147]	29
Fe(salen)cat^-	25.8/29.5	56.5	−33.9	27.0		29
Fe(salpyr)$_2$(MeOH)$_2^+$	18.2	85.7	−80.3	61.0		22
Fe(salen)acac	21.6	75.0	−60.7	45.5		31
Fe(salhis)$_2^+$	18.9	75.9	−65.3	47.3		19
Fe(salen)(N-CH_3Im)$_2^+$	19.9	72.2	−60.4	39.8		32
Fe(salen)Im_2^+	19.8	72.1	−60.4	39.4		33
Fe(sal-*n*-prop)$_2Im_2^+$	19.3	68.6	−67.9	39.0		33
Fe_2(saldap)$_3$	21.2	71.0	−54.3	41.0		34
Fe(sal-*n*-prop)$_2$Cl	21.8	82.9	−69.3	53.2		35
Fe(salps)Cl 0-1	17.9	93.3	−75.1	54.0		36
Fe(salps)Cl 0-2	19.7	86.5	−75.1	49.2		

[a] Obtained in acetone solution. [b] Obtained in acetone-d_6 at 300 K. 4-H, 5-H, and 6-H refer to protons on the salicydenamine ring. [c] Obtained in acetonitrile.

dioxygenases prompted us to explore this further.[19-20] We have studied the absorption maxima, paramagnetic NMR shifts, electrochemical potential, and Raman excitation profiles of a series of iron(III) phenolate complexes and find that the phenolate-to-iron(III) charge-transfer band reflects the strength of the other ligands coordinated to the iron. As the other ligands become weaker, the iron–phenolate interaction becomes stronger, resulting in red-shifted absorption maxima, larger contact shifts, and more positive reduction potentials. On the basis of these studies, we propose that the iron site for the catechol dioxygenases approaches square-pyramidal geometry with an apical and basal phenolate to explain the Raman excitation profiles observed for several dioxygenase complexes.[19,20] Insights into the enzyme–substrate complexes and reaction intermediates of the dioxygenases are also obtained; the observations support the premise that the active site iron remains high-spin ferric during the catalytic cycle.[23,24]

Experimental Section

The model complexes were synthesized following procedures referenced in Table I.[25] Catechol was sublimed prior to use, *p*-cresol was distilled at reduced pressure, and all other materials were reagent grade and used without further purification. Acetonitrile was anaerobically distilled from P_2O_5 immediately before use.

[Fe(salen)]$_2$O was synthesized according to published procedures.[37] Isotopically pure iron was obtained from Oak Ridge National Laboratory as $^{54}Fe_2O_3$. The ferric oxide was dissolved in concentrated nitric acid with gentle heating, filtered through a glass wool plug and evaporated to dryness. The resulting $Fe(NO_3)_3 \cdot xH_2O$ was used to form $Fe_2O_3 \cdot xH_2O$ required for efficient dimer synthesis. Deuterated *p*-cresol-d_5 was obtained via acid exchange at 130 °C for a total of 40 h,[38] with NMR

(17) May, S. W.; Phillips, R. S.; Oldham, C. D. *Biochemistry* **1978**, *17*, 1853–1860.
(18) Kojima, Y.; Fujisawa, H.; Nakazawa, A.; Nakazawa, T.; Kanetsuna, F.; Taniuchi, H.; Nozaki, M.; Hayaishi, O. *J. Biol. Chem.* **1967**, *242*, 3270–3278.
(19) Que, L., Jr.; Heistand, R. H., II; Mayer, R.; Roe, A. L. *Biochemistry* **1980**, *19*, 2588–2593.
(20) Que, L., Jr.; Epstein, R. M. *Biochemistry* **1981**, *20*, 2545–2549.
(21) Ackermann, G.; Hesse, D. *Z. Anorg. Allg. Chem.* **1970**, *375*, 77–86.
(22) Ainscough, E. W.; Brodie, A. M.; Plowman, J. E.; Brown, K. L.; Addison, A. W.; Gainsford, A. R. *Inorg. Chem.* **1980**, *19*, 3655–3663.
(23) Que, L., Jr.; Lipscomb, J. D.; Munck, E.; Wood, J. M. *Biochim. Biophys. Acta* **1977**, *485*, 60–74.
(24) Que, L., Jr.; Lipscomb, J. D.; Zimmermann, R.; Munck, E.; Orme-Johnson, N. R.; Orme-Johnson, W. H. *Biochim. Biophys. Acta* **1976**, *452*, 320–334.
(25) Abbreviations used: salen, *N,N'*-ethylenebis(salicylidenamine) dianion; PD,9,10-phenanthrenediol dianion; cat, 1,2-dihydroxybenzene dianion; DBcat, 3,5-di-*tert*-butylcatechol dianion; salpyr, 2-(5-methylpyrazol-3-yl)-phenol anion; acac, 2,4-pentanedione anion; Im, imidazole; sal-*n*-prop, *N*-*n*-propyl(salcylidenamine) anion; salhis, *N*-[2-(4-imidazolyl)ethyl)]salicylidenamine anion; saldap, *N,N'*-(1,3-propane)bis(salicylidenamine) dianion; salps, *N,N'*-(2,2'-disulfidodiphenyl)bis(salicylidenamine) dianion; CTD, catechol 1,2-dioxygenase; PCD, protocatechuate 3,4-dioxygenase; EXAFS, extended X-ray absorption fine structure; OAc, acetate; Fc^+, ferrocenium cation; Fc, ferrocene; SCE, saturated calomel electrode.
(26) Gulloti, M.; Casella, L.; Pasuni, A.; Ugo, R. *J. Chem. Soc., Dalton Trans.* **1977**, 339–345.
(27) Bancroft, G. M.; Maddock, A. G.; Randl, R. P. *J. Chem. Soc. A* **1968**, 2939–2944.
(28) Gerloch, M.; Mabbs, F. E. *J. Chem. Soc. A* **1967**, 1900–1908.
(29) Heistand, R. H. II; Lauffer, R. B.; Fikrig, E.; Que, L. Jr. *J. Am. Chem. Soc.* **1982**, *104*, 2789–2796.
(30) White, L. S., unpublished results.
(31) Lauffer, R. B.; Heistand, R. H., II; Que, L., Jr. *Inorg. Chem.* **1983**, *22*, 50–55.
(32) Amundsen, A. R.; Whelan, J.; Bosnich, B. *Inorg. Chem.* **1978**, *18*, 206–208.
(33) Nishida, Y.; Oshio, S.; Kida, S. *Bull. Chem. Soc. Jpn.* **1977**, *50*, 119–122.
(34) Heistand, R. H., II Ph.D. Thesis, Cornell University, 1982.
(35) Bergen, A. van Den; Murray, K. S.; O'Connor, M. J.; Rehak, N.; West, B. O. *Aust. J. Chem.* **1968**, *21*, 1505–1515.
(36) Bertrand, J. A.; Breece, J. L. *Inorg. Chim. Acta* **1974**, *8*, 267–272.
(37) Lewis, J.; Mabbs, F. E.; Richards, A. *J. Chem. Soc. A* **1967**, 1014–1018.

showing >90% deuterium incorporation. Enriched *p*-cresol-^{18}O was synthesized by the decomposition of the corresponding diazonium salt in ^{18}O-enriched water.[39] Mass spectral data indicated an ^{18}O isotopic purity of approximately 50%.

Optical spectra of Fe(salen)X complexes were recorded in acetone on a Cary 219 UV–visible spectrophotometer using solutions containing a large enough excess of HX to ensure complete formation of Fe(salen)X.[29] The spectra of other ferric complexes were also obtained directly in acetone.

Paramagnetic NMR spectra were obtained in acetone-d_6 and recorded on a Bruker WM300 spectrometer at 300 K using a 10-μs 90° pulse, a 125-kHz bandwidth, and 8K data points. Chemical shifts were referenced to tetramethylsilane with downfield shifts taken as positive. Peak assignments were made by comparison with closely related complexes.[29,40]

Resonance Raman spectra were obtained by using a Coherent Radiation Model 500K krypton ion laser and Model CR-3 argon ion laser. The spectra were recorded on a SPEX 1401 spectrometer interfaced with a microprocessor for data handling. Spectra were obtained on anaerobic CD_3CN solutions of the complexes using a solvent vibration as reference. Isotopic shifts and line widths were measured by using a least-squares fit in the area of interest.[41] Small isotopic shifts observed for $^{54}Fe/^{56}Fe$ were measured by using a comparison of the line widths of the individual solutions and that of a 1:1 solution containing both isotopes.

Electrochemical measurements were made in acetonitrile with 0.1 M tetraethylammonium perchlorate as electrolyte using a Bioanalytical Systems apparatus. A three-electrode system consisting of a Pt working electrode, a Pt auxiliary electrode, and a $Ag/AgNO_3$ 0.1 M in (CH_3CN) reference electrode was used. Ferrocene was used as an internal standard and potentials are reported referenced to SCE ($E^{o\prime}$ for Fc^+/Fc vs. SCE + 0.155 V).[42]

Results and Discussion

Resonance Raman Studies. Iron phenolate complexes have been used as models for the iron–tyrosinate proteins in a variety of studies.[3,21,22,29] They have been useful for mimicking the electronic absorption spectra and the resonance Raman spectra of the proteins. However the phenolates in these ligands are mostly ortho substituted, which complicates the Raman spectra of these complexes, and renders them less useful for making resonance Raman assignments. For such studies, a *p*-cresolate ligated to a ferric center would be a more appropriate model for iron–tyrosinate proteins.

The synthetic route to such an iron *p*-cresolate complex was developed by Heistand et al.[29] who demonstrated that Fe(salen)phenolate complexes may be obtained by treating $[Fe(salen)]_2O$ with a suitable excess of the desired phenol. The amount of excess required is inversely proportional to the acidity of the phenol. Fe(salen)OC_6H_4-4-CH_3 was generated following this procedure and characterized by its visible and NMR spectra. Its resonance Raman spectrum obtained using 647.1-nm excitation is shown in Figure 1. Both salen and *p*-cresolate vibrations are observed. Features at 617, 1337, and 1450 cm^{-1} are assigned to salen vibrations by comparison with the spectrum of Fe(salen)OAc, while remaining features at 568, 1168, 1272, 1501, and 1602 cm^{-1} are assigned to the *p*-cresolate. With the exception of the 568-cm^{-1} peak, these features are identical with those assigned to tyrosinate vibrations in proteins and constitute the characteristic fingerprint for metal–tyrosinate proteins.[2-13] Thus Fe(salen)OC_6H_4-4-CH_3 serves as a model for iron–tyrosinate proteins for making Raman assignments.

The assignments of the high-frequency vibrations have been made by using normal mode analysis;[4] however, the feature at 568 cm^{-1} remains to be assigned. Similar features have been observed in several iron–tyrosinate proteins and two suggestions for its assignment have been proposed. In studies of uteroferrin, the peak at 575 cm^{-1} has been suggested to arise from coupled

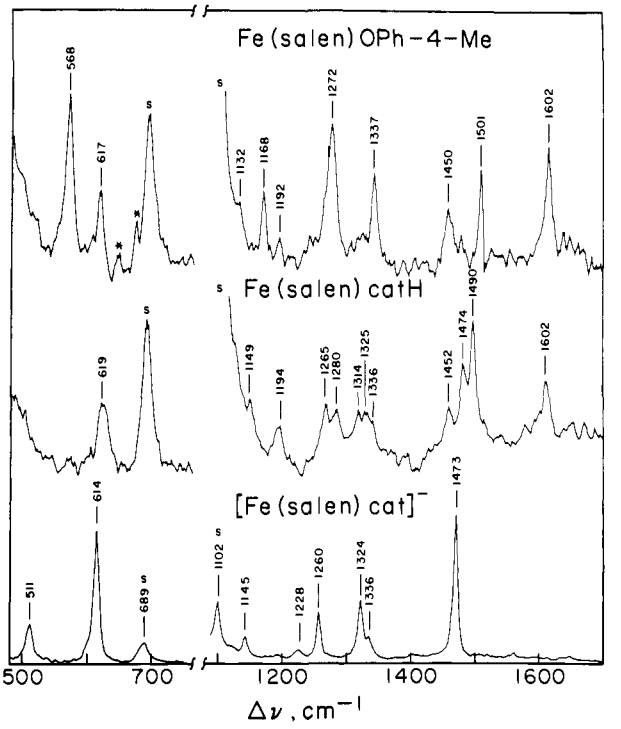

Figure 1. Resonance Raman spectra of Fe(salen)X complexes. Conditions: 647.1-nm excitation, 150-mW power, 4-cm^{-1} slit width, CD_3CN solvent, ~1 mM concentration except for $[Fe(salen)cat]^-$ which had a concentration of ~2 mM.

Fe–O stretches of cis-coordinated tyrosinates.[12] Mutant hemoglobins where histidine has been replaced by tyrosine as the axial ligand also show Raman peaks in this region, at 603 and 588 cm^{-1} for Hb M Boston and Hb M Iwate, respectively; these are suggested to be Fe–O(Tyr) stretches[14] by analogy to the Fe–O stretch for oxyhemoglobin[43,44] and its synthetic analogue[45] found at 568 cm^{-1}.

Because of the ease of isotope substitution into the *p*-cresolate moiety, Fe(salen)OC_6H_4-4-CH_3 provides the opportunity to assign the ca. 570-cm^{-1} feature in the proteins. In the model complex this peak is found at 568 cm^{-1} and is polarized (ρ = 0.30) as expected for a totally symmetric mode.[46] The observation of this feature in the mutant hemoglobins which clearly have only one coordinated tyrosinate argues against the possibility that this feature arises from coupled Fe–O stretches from cis-coordinated tyrosinates. The suggestion that this is an Fe–O stretch can be verified with a study of the complex with ^{54}Fe and ^{18}O substitution and ring deuteration.

For an isolated two-body Fe–O stretch, the $^{54}Fe/^{56}Fe$ shift is calculated to be 2.3 cm^{-1}. Since this was close to the limit of reproducibility for our system, we compared the spectra of three samples—the ^{54}Fe complex, the ^{56}Fe complex, and a 1:1 mixture of the two—and measured the line width of the ca. 570-cm^{-1} feature. The isotopically pure complexes exhibited peaks with nearly identical line widths (7.2 ± 0.1 cm^{-1}), while the mixture exhibited a broader peak (7.9 cm^{-1}). On the basis of Gaussian fits to the peaks, the isotope shift was found to be ca. 0.7 cm^{-1}. ^{18}O substitution of the *p*-cresol oxygen results in a shift of 10 cm^{-1}, to 558 cm^{-1}. A two-body Fe–O stretching model predicts an isotope shift of 25 cm^{-1}. Deuteration of the ring protons of *p*-cresol results in an 8-cm^{-1} shift.

Taken together, the isotope experiments indicate that the feature at ca. 570 cm^{-1} must have some Fe–O stretching character since

(38) Jakobsen, R. J. *Spectrochim. Acta* **1965**, *21*, 433–442.
(39) Pinchas, S.; Sadeh, D.; Samuel, D. *J. Phys. Chem.* **1965**, *69*, 2259–2264.
(40) LaMar, G. N.; Eaton, G. R.; Holm, R. H.; Walker, F. A. *J. Am. Chem. Soc.* **1973**, *95*, 63–75.
(41) #CURFT, least-squares fitting routine adapted for Raman data by Mike Cannarsa, Cornell University, 1982.
(42) Gagne, R. R.; Koval, C. A.; Lisensky, G. *Inorg. Chem.* **1980**, *19*, 2854–2855.
(43) Brunner, H. *Naturwissenschaften* **1974**, *61*, 129.
(44) Nagai, K.; Kitagawa, T.; Morimoto, H. *J. Mol. Biol.* **1980**, *136*, 271–289.
(45) Burke, J. M.; Kincaid, J. R.; Peters, S.; Gagne, R. R.; Collman, J. P.; Spiro, T. G. *J. Am. Chem. Soc.* **1978**, *100*, 6083–6088.
(46) Behringer, J. In "Raman Spectroscopy: Theory and Practice"; Szymanski, H. A., Ed; Plenum Press: New York, 1967; pp 162–180.

Table II. Raman Spectra of Iron–Catecholate Complexes

compd	Raman bands					ref
Fe(salen)catH		619	1265/1280		1474/1490	*a*
Fe(salen)catD-d_5			1197		1428 (br)	*a*
$[Fe(salen)cat]^-$	511	614	1260	1324	1473	*a*
$[Fe(salen)cat\text{-}d_4]^-$		599	1202		1426	*a*
$[Fe(cat)_3]^{3-}$	533	622	1267	1327	1487	*b*
$[Fe(cat\text{-}d_4)_3]^{3-}$		610	1206		1436	*a*

[a] This work. [b] Reference 51.

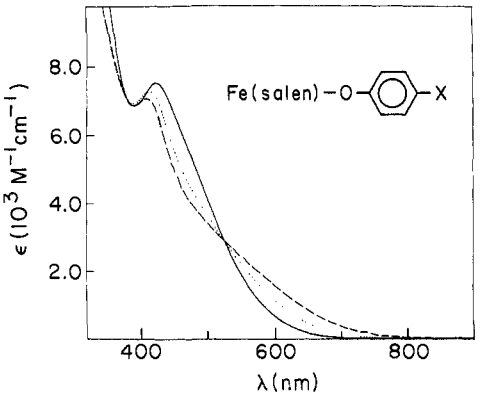

Figure 2. Visible absorption spectra of Fe(salen)phenolate complexes in CH_2Cl_2. X = CN (—), Cl (···), CH_3 (- - -).

it is sensitive to the iron isotope. However, it must also have tyrosine ring character. The ν_{12} (benzene notations)[47] mode observed in *p*-cresol at 738 cm^{-1} is the only candidate in the region of interest, since the polarization experiments indicate the ca. 570-cm^{-1} vibration to be a symmetric mode. The ν_{12} mode is sensitive to the nature of the 1- and 4-substituents of the benzene ring and exhibits substantial ^{18}O and deuteration shifts.[38,48,49] The ν_{6a} mode of *p*-cresol at 464 cm^{-1} was also considered, but it seemed unlikely that the band would shift to higher frequency upon iron coordination. We thus favor the assignment of the ca. 570-cm^{-1} feature as a vibrational mode consisting of an Fe–O stretch and ν_{12}.

We have also studied the resonance Raman properties of Fe(salen)catH and $[Fe(salen)cat]^-$, synthetic iron complexes with monodentate[50] and chelated[31] catecholates, respectively. Their Raman spectra, obtained with 647.1-nm excitation, are shown in Figure 1. With 647.1 nm excitation, the dominant features arise from catecholate vibrations, easily assigned by ring deuteration (Table II). For $[Fe(salen)cat]^-$, all the observed features match those reported for other chelated catecholate complexes.[8,51] Fe(salen)catH exhibits catecholate vibrations which are similar to those of the chelated complex in energies; the features, however, are doubled as expected for an ortho-substituted phenol.[48] The two catecholate complexes also differ in the low-frequency region. The chelated complex exhibits a feature at 509 cm^{-1} which is not observed in the monodentate complex. This compares well with features observed for $[Fe(cat)_3]^{3-}$ [51] and $[Fe(oxalate)_3]^{3-}$ [52] at 533 and 528 cm^{-1}, respectively. A normal coordinate analysis of the oxalate complex has assigned this band as a mode intrinsic to the five-membered ring upon chelation of the oxalate to the iron[52] and this assignment has been extended to the catecholate complexes.[51]

(47) Varsanyi, G.; Szoke, S. "Vibrational Spectra of Benzene Derivatives"; Academic Press: New York, 1979.
(48) Green, J. H. S.; Harrison, D. J.; Kynaston, W. *Spectrochim. Acta* **1971**, *27A*, 2199–2217.
(49) Cummings, D. L.; Wood, J. L. *J. Mol. Struct.* **1974**, *20*, 1–40.
(50) Heistand, R. H. II; Roe, A. L.; Que, L. Jr. *Inorg. Chem.* **1982**, *21*, 676–681.
(51) Salama, S.; Stong, J. D.; Neilands, J. B.; Spiro, T. G. *Biochemistry* **1978**, *17*, 3781–3785.
(52) Nakamoto, K. "Infrared Spectra of Inorganic and Coordination Compounds"; Wiley-Interscience: New York, p 245.

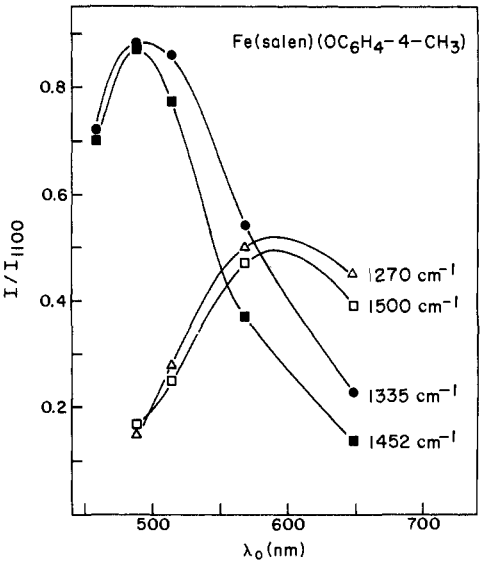

Figure 3. Excitation profile for $Fe(salen)(OC_6H_4\text{-}4\text{-}CH_3)$ in CD_3CN. Complex was ~1 mM in concentration. Peak heights were normalized relative to the 1102-cm^{-1} band of CD_3CN.

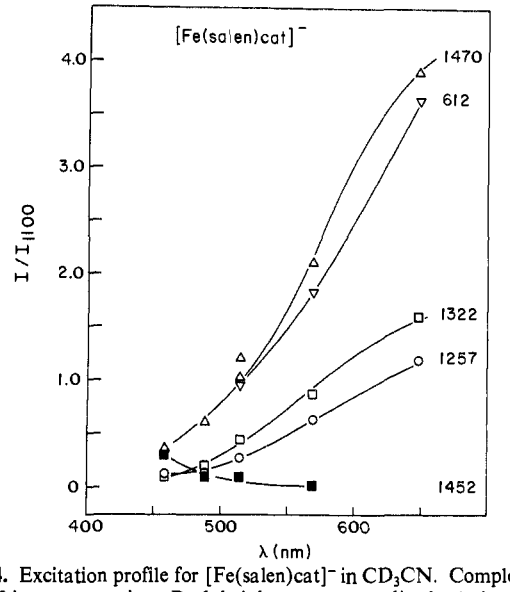

Figure 4. Excitation profile for $[Fe(salen)cat]^-$ in CD_3CN. Complex was ~2 mM in concentration. Peak heights were normalized relative to the 1102-cm^{-1} band of CD_3CN.

Factors Affecting Phenolate-to-Iron(III) Charge Transfer. A series of high-spin ferric phenolate complexes has been investigated in order to clarify the factors that affect the energy of the phenolate-to-iron(III) charge-transfer transition. Visible and NMR spectra as well as cyclic voltammograms have been obtained for these complexes and the results are summarized in Table I. Resonance Raman excitation profiles for three of these complexes have also been obtained to clarify the electronic transitions in these complexes.

The series consists of iron complexes with two coordinated salicylidenamines and variable fifth and sixth ligands. The complexes studied exhibit visible spectra with absorbance maxima which span the range of 339–640 nm. Visible spectra for some Fe(salen)phenolates are shown in Figure 2. They exhibit spectral shapes and extinction coefficients typical of the series. The phenolate complexes exhibit absorbance maxima near 420 nm, with the exact position being a function of the nature of the substituent on the axial phenolate. As X varies from CH_3 to CN, the absorbance maximum red shifts and the long wavelength tail recedes. To further understand these spectra, the excitation profile of $Fe(salen)OC_6H_4\text{-}4\text{-}CH_3$ was obtained (Figure 3). The profile shows that the salen and *p*-cresolate vibrations are maximally

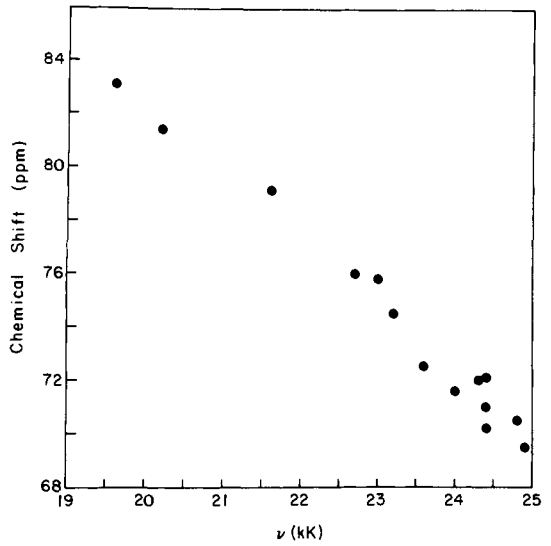

Figure 5. Plot of the 4-H chemical shifts in Fe(salen)X complexes vs. the absorbance maxima of the complexes.

enhanced near 500 and 600 nm, respectively, indicating the presence of two transitions arising from salen-to-iron(III) and *p*-cresolate-to-iron(III) charge transfer. The visible spectra are interpreted to indicate the axial phenolate-to-iron(III) charge-transfer blue shifts as the phenolate becomes more electron withdrawing, while the salen-to-iron(III) transition red shifts. Fe(salen)catH which exhibits a visible spectrum[29] similar to those of Fe(salen)phenolates also gives rise to a similar excitation profile. In this complex, the catecholate vibrations are maximally enhanced near 600 nm.

[Fe(salen)cat]$^-$, on the other hand, exhibits a visible spectrum with maxima at 339, 388, and 628 nm.[29] The excitation profile of this complex (Figure 4) also reveals the presence of two phenolate-to-iron(III) charge-transfer transitions. Catecholate vibrations are maximally enhanced near 650 nm, thus assigning the 628-nm feature to the catecholate-to-iron(III) charge-transfer band. The salen-to-iron(III) charge-transfer band is clearly in the near UV, since salen vibrations are not observed in the Raman spectra of this complex except with the lowest wavelength excitation available. The data available are not sufficient to assign it to the 339- or 388-nm band. The important observation here is that the salen charge-transfer band dramatically shifts to higher energy upon chelation of catechol.

The complexes studied exhibit proton NMR spectra with features outside the diamagnetic region due to the presence of the $S = {}^5/_2$ center. Because of the near spherical distribution of the electrons in such a center, the paramagnetic shifts observed are predominantly, if not solely, contact in origin; i.e., they arise from the delocalization of unpaired spin density onto the ligand.[53] Previous NMR studies on paramagnetic Schiff base complexes have shown that unpaired spin density is delocalized via a π mechanism, resulting in an alternation in the sign of the contact shift exhibited by the ortho, meta, and para protons of the phenolate moiety;[29,40] this is indeed observed for our complexes. Figure 5 shows that, in a series of five-coordinate Fe(salen) complexes, the salen contact shifts become larger as the energy of the salen-to-iron(III) charge-transfer band shifts to lower energy. This correlation clearly demonstrates that the charge-transfer interaction provides the mechanism for the delocalization of unpaired spin density onto the ligand.[53] The lower the energy of the charge-transfer band, the greater the extent of mixing between the iron d and phenolate orbitals, the larger the shifts observed. Our limited number of six-coordinate salicylaldimine complexes also shows this general trend. For example, [Fe(salen)cat]$^-$ has the highest energy salen-to-iron(III) charge-transfer and the smallest NMR shifts, while Fe(salpyr)$_2$(MeOH)$_2^+$ with the lowest energy charge-transfer band shows one of the largest NMR shifts.

The NMR spectra of the square-pyramidal Fe(salen)-OC_6H_4-4-X complexes exhibit resonances from both salen and the axial phenolate; these resonances shift in qualitative agreement with the correlation of shift vs. absorbance maxima. As X becomes more electron withdrawing,[54] i.e., the axial phenolate becomes a poorer ligand, the salen contact shifts increase in consonance with the red shift of the absorbance maximum. Simultaneously, the contact shifts for the axial phenolate decrease in agreement with the blue shift of the long wavelength tail in the visible spectra (Figure 2). These observations indicate that the salen ligand compensates for the weaker axial ligand by bonding more strongly to the metal. Conversely, in a series of complexes with constant axial ligand and substituted salens, the NMR shifts of the axial ligand increase as the substituents on the salen become more electron withdrawing, while the salen shifts decrease (Table III). Thus the axial ligand is also sensitive to changes in the complex. So, by varying the strengths of the other ligands in an iron–phenolate complex, one can in principle shift the energy of the charge-transfer band over a wide spectral range.

Table III. NMR Shifts of Fe(salen)phenolate Complexes[a]

complex	4-H	*o*-H	*m*-H
Fe(3-OCH_3-salen)phenolate			
2,4,6-Cl_3	80.4		72.4
4-CN	75.4	72.8	75.3
4-CF_3	77.9	79.2	77.9
4-Cl	77.3	90.2	81.6
4-OCH_3	76.6	n.o.	83.0
Fe(salen)phenolate			
2,4,6-Cl_3	74.5		72.4
4-CN	72.5	-72.7	77.3
4-CF_3	72.0	-81.0	78.5
4-Cl	71.0	-92.4	82.4
4-OCH_3	69.5	-107.9	84.1
Fe(5-Cl-salen)phenolate			
2,4,6-Cl_3	70.9		75.2
4-CN	68.6	-77.1	78.3
4-CF_3	68.1	-84.6	80.7
4-Cl	67.3	-95.7	84.7
4-OCH_3	64.4	-114.2	84.8

[a] NMR spectra obtained in acetone-d_6 at 300 K. Chemical shifts referenced to $(CH_3)_4Si$ with downfield shifts taken as positive. 4-H refers to salen 4-H proton and *o*-H and *m*-H refer to protons on the axial phenolate.

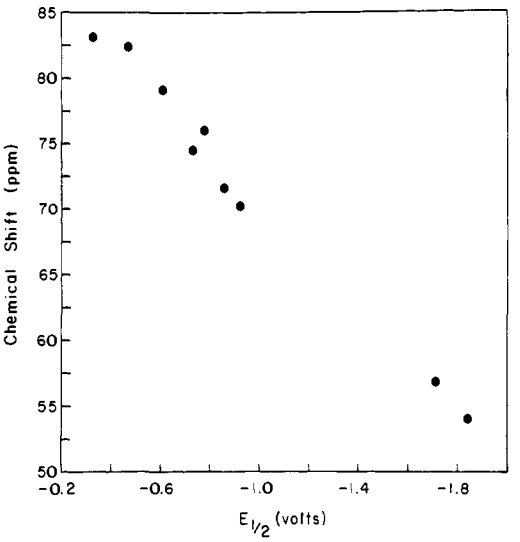

Figure 6. Plot of the 4-H chemical shifts in Fe(salen)X complexes vs. the Fe^{III}/Fe^{II} potentials of the complexes.

(53) LaMar, G. N. In "NMR of Paramagnetic Molecules, Principles and Applications"; LaMar, G. N., Horrocks, W. D., Holm, R. H., Eds.; Academic Press: New York, 1973; Chapter 3. Horrocks, W. D., Jr. Ibid.; Chapter 4.

(54) A Hammett plot of the salen 4-H shift vs. σ_p for the 4-X substituent on the axial phenolate gives a straight line with $\rho = 3.43$ and a correlation coefficient of 0.996.

Complexes representative of the series were also investigated electrochemically (Table I). They all exhibited quasi-reversible cyclic voltammograms with the exception of the catecholate complexes which showed some dissociation of the catecholates upon reduction. The Fe^{III}/Fe^{II} redox potential correlates well with the energy of the salen-to-Fe(III) charge-transfer band as reflected by the NMR contact shifts (used in the correlations because of the greater accuracy of determination) (Figure 6). As the ligand field strength of the variable ligand increases, the redox potential shifts to more negative values. The correlation suggests that changes in the energy of the $d\pi$ orbitals in the ferric complex are a major determinant of the redox potential, because the energy of the charge-transfer band reflects the larger variations of the energy of the ferric $d\pi$ orbitals relative to the essentially invariant phenolate $p\pi$ orbitals. The variation in the Fe^{III}/Fe^{II} reduction potential is also a function of the Fe(II) complex but the variations in the ferrous complexes are expected to be smaller, since the axial ligand is not likely to have a high affinity for Fe^{II}(salen).

Taken together, the visible, NMR, and electrochemical data give rise to the following spectrochemical series for Fe(salen)X complexes in order of increasing ligand strength: $I^- < Br^- < Cl^- < PhS^- \sim AcO^- < PhO^- < cat^{2-}$. A similar order is reported for a study of $[FeX_4]^-$ complexes.[55] Our observations indicate that the properties of the iron phenolate moiety are sensitive to the strength of the other ligands coordinated in the same complex. When a ligand is replaced by a weaker donor, the iron–phenolate interaction becomes stronger as indicated by the larger NMR shifts, the lower energy charge-transfer band, and the more positive potentials. These generalizations are also consistent with previously reported observations by Ainscough et al.[22] Among the oxygen ligands, the series appears to follow an order of increasing basicity; the more basic the ligand the more blue-shifted the salen-to-iron(III) charge-transfer transition. Interestingly, $[Fe(salen)]_2O$ appears to follow this trend, exhibiting a salen-to-iron(III) charge-transfer band in the near ultraviolet, consistent with the rather basic oxide ligand. Unfortunately, the strong antiferromagnetic coupling in the binuclear complex prevents its inclusion in our studies.[56]

In the course of our studies, we have investigated the spectroscopic properties of Fe(salps)Cl which is of particular importance for understanding the active site structure of the catechol dioxygenases. The ligand derived from the condensation of salicylaldehyde and 2,2′-diaminodiphenyl disulfide is potentially tetra-, penta-, or hexadentate. The crystal structure of the chloride has been reported[36] and a schematic diagram is shown. The ligand is pentadentate in this complex with only one of the disulfide sulfurs coordinated. The complex is best described as a square pyramid with a weak sixth intereaction. The Fe–S distance is long (2.54 Å) but not unexpected for an iron–disulfide interaction. The Fe–O bond trans to the sulfur is shorter (1.87 Å) relative to the other Fe–O bond (1.91 Å). Comparisons with other square-pyramidal complexes indicate that the Fe–O bond lengths for the two phenolates are typical of those observed for apical and basal phenolates, respectively.[50,57] Two sets of salicylyl NMR resonances of equal intensity are observed for this complex, and two visible maxima are discernible at ca. 510 and 560 nm, clearly indicating the presence of two charge-transfer bands. On the basis of our studies, the apical phenolate would be associated with the lower energy transition and the basal phenolate the higher energy transition. We suggest that this results from the differing strengths of the iron–phenolate interactions, manifested in the difference in Fe–O bond lengths. This example demonstrates that it is possible to constitute a complex having two identical phenolate ligands but having different phenolate-to-iron(III) charge-transfer energies.

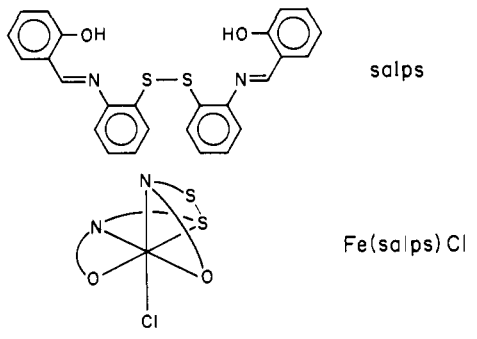

Insights into the Catechol Dioxygenases. Our studies provide several insights into the coordination chemistry of the iron center in the catechol dioxygenases. We have already noted the similar trends in the λ_{max}'s between Fe(salen)X complexes and corresponding CTD–X and PCD–X complexes.[29] This correspondence indicates that the factors affecting the salen-to-iron(III) charge-transfer transition also apply to the tyrosinate-to-iron(III) charge-transfer transition in the dioxygenases. One intriguing puzzle has been the observation by resonance Raman spectroscopy of two tyrosinate-to-iron(III) charge-transfer bands in several dioxygenase complexes. These complexes exhibit tyrosine excitation profiles[19,20] whose maxima are separated by 2000–4000 cm^{-1}. Since the two tyrosines would be expected to be rather similar, the two charge-transfer transitions must be a result of differing iron–phenolate interactions. On the basis of our model studies, we would suggest that the dioxygenase active site has a geometry approaching that of a square pyramid where one tyrosine occupies an apical position and the other a basal position. The apical tyrosine would be expected to have the shorter Fe–O bond and give rise to the lower energy charge-transfer band, as modeled by Fe(salen)OC_6H_4-4-CH_3 and Fe(salps)Cl. Such a configuration is consistent with conclusions derived from X-ray absorption pre-edge studies. These studies indicate that the dioxygenases in general have coordination numbers intermediate between five and six coordinate.[58] One structure consistent with these observations is shown as follows:

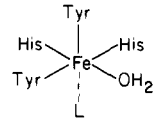

The proposed structure is a six-coordinate complex where a weak sixth ligand is trans to one tyrosine. This would result in the shortening of that particular Fe–O(tyrosine) bond as observed for Fe(salps)Cl. The participation of histidine in the iron coordination has been suggested by EXAFS studies,[59] while the involvement of water has been demonstrated by EPR studies in $H_2{}^{17}O$.[60,61] The latter studies, together with the effects of cyanide ligation,[60,61] suggest the presence of two available, probably adjacent, sites on the iron center, as depicted by the diagram.

The model studies are also relevant to the spectral changes observed upon substrate binding. Resonance Raman studies of the ES complexes of CTD and PCD show the presence of both tyrosinate- and catecholate-to-iron(III) charge-transfer bands. The binding of substrate introduces a new feature in the visible spectrum of the enzyme at 600–800 nm, which is assigned to catecholate.[8,9] The binding of catecholate shifts the tyrosinate-to-iron(III) charge-transfer band to higher energy. The tyrosinate vibrations, observed with 647.1-nm excitation in the native enzymes, are observed in the ES complexes only with excitation at shorter wavelengths, e.g., 514.5 nm.[8,9,62] Certain spectral

(55) Koch, S. A.; Millar, M. *J. Am. Chem. Soc.* **1982**, *104*, 5255–5257.
(56) Murray, K. S.; *Coord. Chem. Rev.* **1974**, *12*, 1–36.
(57) Goff, H. M.; Shimomura, E. T.; Lee, Y. J.; Scheidt, W. R. *Inorg. Chem.* **1984**, *23*, 315–321.
(58) Roe, A. L.; Schneider, D. J.; Mayer, R. J.; Pyrz, J. W.; Widom, J.; Que, L., Jr. *J. Am. Chem. Soc.* **1984**, *106*, 1676–1681.
(59) Felton, R. H.; Barrow, W. L.; May, S. W.; Sowell, A. L.; Goel, S. *J. Am. Chem. Soc.* **1982**, *104*, 6132–6134.
(60) Lipscomb, J. D.; Whittaker, J. W.; Arciero, D. M. In "Oxygenases and Oxygen Metabolism"; Nozaki, M., Yamamoto, S., Ishimura, Y., Coon, M. J., Ernster, L., Estabrook, R. W., Eds.; Academic Press: New York, 1982; pp 27–38.
(61) Whittaker, J. W.; Lipscomb, J. D. *J. Biol. Chem.* **1984**, *259*, 4487–4495.

properties of the ES complexes are mimicked by synthetic complexes with either monodentate and chelated catecholate. Catecholate-to-iron(III) charge-transfer transitions are observed near 600 nm and catecholate binding results in blue shifts of the salen-to-iron(III) charge-transfer band. However, neither model complex adequately reproduces the spectral properties observed for the enzyme complexes. Though the Raman spectra of the ES complexes are modeled well by [Fe(salen)cat]$^-$, the excitation profiles of the ES complexes are better matched by that of Fe(salen)catH. Thus resonance Raman data to date cannot distinguish the mode of catechol binding to the enzymes. The catecholate coordination mode in the ES complexes has been elucidated by using paramagnetic NMR spectroscopy based on the same models. The catecholate was found to be monodentate in the CTD ES complex and chelated in the PCD ES complex.[63]

Our model studies support the proposed dioxygenase reaction mechanism, which does not involve the ferrous oxidation state.[23] Mössbauer spectroscopy has conclusively shown that no ferrous species can be discerned in the native enzymes, the enzyme–substrate complexes, and the steady-state intermediates generated from PCD, 3,4-dihydroxyphenylpropionate, and O_2[24] and from CTD, pyrogallol, and O_2.[64] The presence of tyrosine ligands makes the possibility of the fleeting participation of iron(II) in the reaction cycle quite unlikely. Phenolate ligands favor the ferric oxidation state and lower the Fe^{III}/Fe^{II} reduction potential. The coordination of catecholate, whether as a monodentate or chelated ligand, introduces yet another phenolate moiety into the iron coordination sphere and further lowers the potential. The blue shift of the tyrosinate-to-iron(III) charge-transfer band observed upon substrate binding to the enzymes is indicative of the lowered potential. In addition, intermediates observed in rapid kinetic studies of the catechol dioxygenases all exhibit visible spectra which indicate the persistence of the tyrosinate-to-iron(III) charge-transfer transition throughout the cycle.[64-66] The substantial blue shifts exhibited by some of these complexes suggest structures for the organic intermediates involved in the reaction. When the ES complex is exposed to oxygen, the catecholate charge-transfer band disappears, while the blue-shifted tyrosinate band is retained.[64-66] Since the tyrosinate-to-iron(III) charge-transfer bands of the catechol dioxygenase complexes appear to shift according to the spectrochemical series derived for the model series,[29] the blue shift observed for the first intermediate indicates that the catecholate has been converted to a fairly basic ligand, which would be consistent with alkoxide or peroxide species in the proposed mechanism.[23] Similar blue shifts have been reported for the binding of 2-hydroxypyridine *N*-oxides to PCD and CTD; these substrate analogues are proposed to mimic the ketonized form of the substrate and the blue shift is suggested to result from the binding of the *N*-oxide to the iron.[67,68]

In conclusion, our model studies have provided useful insights into the coordination chemistry of iron–phenolate complexes. We have applied these to the understanding of the active site and mechanism of the catechol dioxygenases. They should also be helpful in interpreting the spectral properties of other iron–tyrosinate proteins.

Acknowledgment. This work was supported by grants from the National Institutes of Health and the National Science Foundation. L.Q. is a Fellow of the Alfred P. Sloan Foundation (1982–1986) and the recipient of an NIH Research Career Development Award (1982–1987). We thank R. H. Heistand, R. B. Lauffer, and especially Professor Harry B. Gray for valuable discussions.

(62) Que, L., Jr., unpublished observations.
(63) Lauffer, R. B.; Que, L., Jr. *J. Am. Chem. Soc.* **1982**, *104*, 7324–7325.
(64) Que, L., Jr.; Mayer, R. *J. Am. Chem. Soc.* **1982**, *104*, 875–877.
(65) Bull, C.; Ballou, D. P.; Otsuka, S. *J. Biol. Chem.* **1981**, *256*, 12681–12686.
(66) Walsh, T. A.; Ballou, D. P.; Mayer, R.; Que, L, Jr. *J. Biol. Chem.* **1983**, *258*, 14422–14427.
(67) May, S. W.; Oldham, C. D.; Mueller, P. W.; Padgette, S. R.; Sowell, A. L. *J. Biol. Chem.* **1982**, *257*, 12746–12751.
(68) Whittaker, J. W.; Lipscomb, J. D. *J. Biol. Chem.* **1984**, *259*, 4476–4486.

Kinetics and Thermodynamics of Intra- and Intermolecular Carbon–Hydrogen Bond Activation

William D. Jones* and Frank J. Feher

Contribution from the Department of Chemistry, University of Rochester, Rochester, New York 14627. *Received May 21, 1984*

Abstract: The preference for intra- and intermolecular C–H bond activation has been determined by equilibration of the complex $(C_5Me_5)Rh(PMe_2CH_2C_6H_5)(C_6H_5)H$ and its cyclometalated analogue $(C_5Me_5)\overline{Rh(PMe_2CH_2C_6H_4)}H$ in neat benzene at 51.2 °C (K_{eq} = 36.7, $\Delta G°$ = −2.32 kcal/mol). By monitoring the approach to equilibrium over a 40 °C temperature range, the difference between the activation parameters for intra- and intermolecular activation by the 16-electron intermediate $[(C_5Me_5)Rh(PMe_2CH_2C_6H_5)]$ can be obtained (intra–inter): $\Delta\Delta H^‡$ = 1.7 ± 0.8 kcal/mol; $\Delta\Delta S^‡$ = 4.5 ± 2.5 eu. At 25 °C, this corresponds to a 1.86:1 kinetic preference for intermolecular activation of the neat benzene solvent by the coordinatively unsaturated intermediate $[(C_5Me_5)Rh(PMe_2CH_2C_6H_5)]$ over intramolecular cycloaddition. The effect of solvent concentration on activation selectivity is discussed. A comparison with intra- and intermolecular alkane activation is made by equilibrating the complex $(C_5Me_5)\overline{Rh(PMe_2CH_2CH_2CH_2)}H$ with benzene and by examining the kinetics of cyclometalation vs. alkane activation. These studies reveal the same general trend with regard to thermodynamic and kinetic selectivity in alkanes and arenes: while there is little kinetic selectivity between intra- and intermolecular reactions involving neat solvent, there is a moderate thermodynamic preference for the intramolecular activation.

The activation of carbon–hydrogen bonds by homogeneous transition-metal complexes is a topic that has received a great deal of attention recently. Much of this interest arises from the recent reports that indicate that even the C–H bonds of alkanes can

0002-7863/85/1507-0620$01.50/0